Analytical Modeling of Magnetic Field Distribution in Spoke-Type Permanent-Magnet Machines

Ali Jabbari[1], Assistant professor, Frédéric Dubas[2], Assistant professor

[1] Sardasht Square, Mec. Eng. Dep., Arak University, Arak, Iran
a-jabbari@araku.ac.ir

[2] Département ENERGIE, FEMTO-ST, CNRS, Univ. Bourgogne Franche-Comté, F90000 Belfort, France
FDubas@gmail.com

Abstract:

A two-dimensional (2-D) analytical method for magnetic field and electromagnetic torque calculation in high-speed spoke-type interior permanent-magnet (PM) machines considering slotting effects, magnetization orientation and winding layout has been proposed in this paper. The analytical method is based on the formal resolution of Laplace's and Poisson's equations as well as the Maxwell's equations in polar coordinate by using subdomain technique and applying hyperbolic functions. The proposed method is applied on the performance computation of a prototype spoke-type PM machine (i.e., a 3-phases 18S-8P motor). The analytical results are validated through 2-D finite-element method (FEM) and experimental tests.

Keywords: Spoke-type motor, Analytical modeling, Subdomain technique, Numerical, Experimental validation.

Submission date : 28 , 10 , 2017

Acceptance date : 21 , 01 , 2019

Corresponding author : Ali Jabbari

Corresponding author’s address: Sardasht Square, Mech. Eng. Dep., Arak University, Arak, Iran.

1. Introduction

Interior PM machines are interested in industrial applications, especially in the electric vehicle due to their high efficiency, power density and robustness [1]. An accurate prediction of air-gap magnetic field distribution is necessary in order to calculate electromagnetic torque, back electromotive force (EMF) and self- or/and mutual inductances more precise. A variety of techniques including analytical and numerical methods has been conducted to evaluate the magnetic field distribution in electrical machines. Numerical methods like FEM give accurate results and are time consuming specially in first step of design stage [2]-[3]. Analytical methods including conformal mapping [4]-[7], magnetic equivalent circuit [8]-[13], Maxwell/Fourier method [14]-[50] and slot relative permeance calculation [51]-[52] are reported to model electrical machines and are useful in first step of performance evaluation and design optimization stage. The inaccuracy of conformal mapping method in modeling of magnetic field distribution in spoke-type PM machines is due to the presence of a deep and small thickness of PM domain. The subdomain technique is more accurate than the other analytical models [8]. It is interesting to note that the saturation effects can be taken into account of this model type [45]-[46]. This method is based on the formal resolution of Laplace's and Poisson's equations in different regions by applying boundary conditions (BCs) for electrical machines [14]-[50].

To author' knowledge, a few analytical models are presented to calculate magnetic field in spoke-type PM machines using subdomain technique [29]-[33]. The novelty and contribution of the manuscript compared to other works is to propose a straightforward expression for magnetic vector potential by using hyperbolic functions. No references in the literature addressing the issue of experimental verification of analytical model for high-speed spoke-type PM machines were found.

The focus of this paper is to develop an analytical model based on the formal resolution of Laplace's and Poisson's equations in multiphase spoke-type PM machines by using the subdomain technique considering slotting effects, magnetization orientation and winding layout. It is shown that the developed model can effectively estimate magnetic field, electromagnetic torque, back-EMF and self-/mutual inductances. This model is applied on the performance calculation of a prototype spoke-type PM motor (i.e., a 3-phases 18S-8P motor). It is shown that the results of analytical model are in close agreement with the results of FEM and experimental tests.

2. Subdomain Definition

The schematic representation of investigated machine is shown in Fig. 1. The machine model is divided into six subdomains. The stator which has two subdomains including Q_1 slot regions (domain m) and Q_1 slot opening regions (domain l) and the air-gap subdomain (region I) are shown in Fig. 2. The rotor has three subdomains including Q_2 inner slot regions (domain i), Q_2 PM regions (domain j), and Q_2 slot-opening regions (domain k), as shown in Fig. 3.

The angular position of the i-th stator slot, i-th stator slot-opening, i-th rotor slot-opening, PM and inner slot are defined as (1), (2), (3) and (4), respectively.

$$\theta_m = -\frac{\alpha}{2} + \frac{2i\pi}{Q_1} \quad \text{with} \quad 1 \le i \le Q_1 \qquad (1)$$

$$\theta_l = -\frac{\beta}{2} + \frac{2i\pi}{Q_1} \quad \text{with} \quad 1 \le i \le Q_1 \qquad (2)$$

$$\theta_k = -\frac{\gamma}{2} + \frac{2i\pi}{Q_2} \quad \text{with} \quad 1 \le i \le Q_2 \qquad (3)$$

$$\theta_i = -\frac{\delta}{2} + \frac{2i\pi}{Q_2} \quad \text{with} \quad 1 \le i \le Q_2 \qquad (4)$$

The following assumptions are made in theoretical analysis:

- Permeability of rotor and stator cores are infinite;
- End effects are neglected.

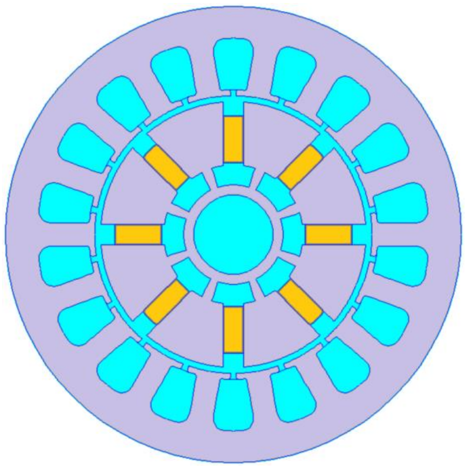

Fig. 1. The geometrical representation of investigated machine.

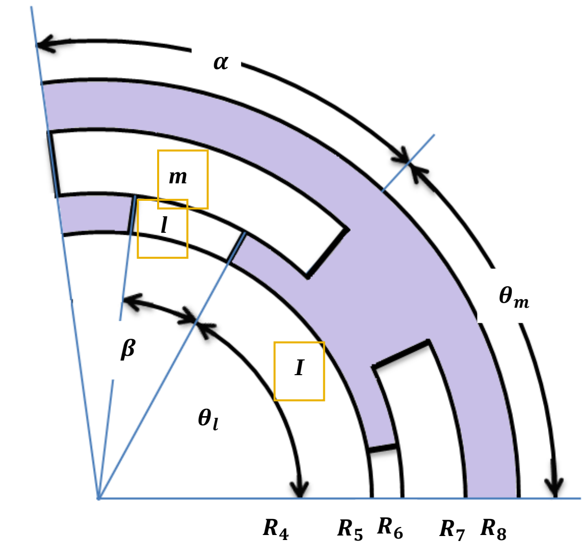

Fig. 2. The stator subdomains including l and m regions.

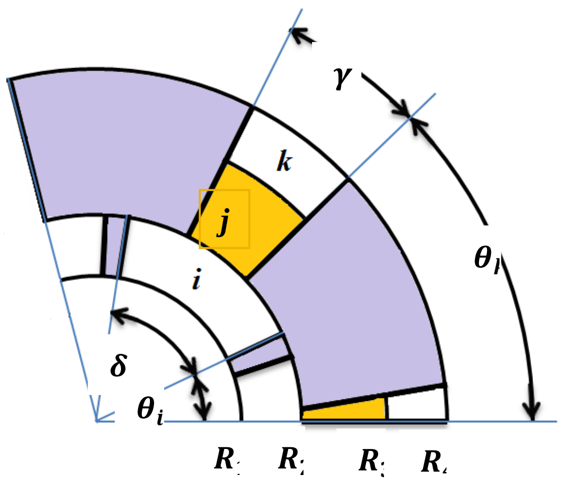

Fig. 3. The rotor subdomains includingi, j and k regions.

3. Magnetic vector potential calculation

General solution of Laplace's or Poisson's equations in each subdomain is developed in this section. The Laplace equation can be described in polar form as

$$\frac{\partial^2 A}{\partial r^2}+\frac{1}{r}\frac{\partial A}{\partial r}+\frac{1}{r^2}\frac{\partial^2 A}{\partial \theta^2}=0 \quad \text{for} \quad \begin{cases} R_1 \le r \le R_2 \\ \theta_1 \le \theta \le \theta_2 \end{cases} \qquad (5)$$

Replacing r by $R_1 e^{-t}$, one obtains

$$\frac{\partial^2 A}{\partial t^2}+\frac{\partial^2 A}{\partial \theta^2}=0 \qquad \text{for} \qquad \begin{cases} ln(\frac{R_1}{R_2}) \le t \le 0 \\ \theta_1 \le \theta \le \theta_2 \end{cases} \qquad (6)$$

3.1. Magnetic Vector Potential in the Stator Slot Subdomain (Region m)

The Poisson's equation in the stator inner slot subdomain is given by

$$\frac{\partial^2 A_m}{\partial t^2}+\frac{\partial^2 A_m}{\partial \theta^2}=-\mu_0 J \text{ for} \begin{cases} t_1 \le t \le t_2 \\ \theta_m \le \theta \le \theta_m+\alpha \end{cases} \qquad (7)$$

where $\boldsymbol{t_1 = ln\left(\frac{R_6}{R_7}\right)}$ and $\boldsymbol{t_2 = 0}$.

Neumann BCs at the bottom and at each side of the slot are obtained as

$$\left.\frac{\partial A_i}{\partial \theta}\right|_{\theta=\theta_m}=0 \qquad \text{and} \qquad \left.\frac{\partial A_i}{\partial \theta}\right|_{\theta=\theta_m+\alpha}=0 \qquad (8)$$

$$\left.\frac{\partial A_i}{\partial t}\right|_{t=t_1}=0 \qquad (9)$$

The general solution of (7) using the separation of variables method is given by

$$A_m(t.\theta)=a_0{}^m-\frac{1}{2}\mu_0 J_i\left(e^{-t_1}t+\frac{1}{2}e^{-2t+t_1}\right) +\sum_{h=1}^{\infty}\left(a_h{}^m\frac{\alpha}{h\pi}\frac{Cosh\left(\frac{h\pi}{\alpha}(t-t_1)\right)}{Sinh\left(\frac{h\pi}{\alpha}(t_2-t_1)\right)}\right). Cos\left(\frac{h\pi}{\alpha}(\theta-\theta_m)\right) \qquad (10)$$

where h is a positive integer, the coefficients $a_0{}^m$and $a_h{}^m$ are determined based on the continuity and interface conditions and

$$J_i(\theta)=J_{i,0}+\sum_{h=1}^{\infty}J_{i,h}cos\left(\frac{h\pi}{\alpha}(\theta-\theta_m)\right) \qquad (11)$$

with

$$J_{i,0}=\frac{1}{2}(J_{1i}+J_{2i}) \qquad (12)$$

$$J_{i,h}=\frac{2}{h\mu}[J_{1i}+(-1)^h J_{2i}]sin\left(\frac{h\pi}{2}\right) \qquad (13)$$

The continuity of the magnetic vector potential between the sub-domain m and the region l leads to

$$\left.\frac{\partial A_m}{\partial t}\right|_{t=t_2} = f(\theta) = \begin{cases} \left.\frac{\partial A_l}{\partial t}\right|_{t=t_3} & for \quad \theta_l \le \theta \le \theta_l + \beta \\ 0 & elsewhere \end{cases} \tag{14}$$

Interface condition (14) gives

$$\mu_0 J_i Sinh(t_1) = \frac{1}{\alpha}\int_{\theta_m}^{\theta_m+\alpha} f(\theta).d\theta \tag{15}$$

$$a_h{}^m = \frac{2}{\alpha}\int_{\theta_m}^{\theta_m+\alpha} f(\theta). Cos\left(\frac{h\pi}{\alpha}(\theta-\theta_m)\right).d\theta \tag{16}$$

3.2. Magnetic Vector Potential in the Stator Slot-Opening Subdomain (Region l)

The Laplace's equation in the stator second inner slot-opening subdomain is given by

$$\frac{\partial^2 A_l}{\partial t^2} + \frac{\partial^2 A_l}{\partial \theta^2} = 0 \quad \text{for} \quad \begin{cases} t_3 \le t \le t_4 \\ \theta_l \le \theta \le \theta_l + \beta \end{cases} \tag{17}$$

where $\mathbf{t_3} = \mathbf{ln}\left(\frac{\mathbf{R_5}}{\mathbf{R_6}}\right)$ and $\mathbf{t_4} = \mathbf{0}$.

Neumann BCs at the bottom and at each side of the slot are obtained as

$$\left.\frac{\partial A_l}{\partial \theta}\right|_{\theta=\theta_l} = 0 \quad \text{and} \quad \left.\frac{\partial A_l}{\partial \theta}\right|_{\theta=\theta_l+\beta} = 0 \tag{18}$$

The general solution of (17) using the separation of variables method is given by

$$A_l(t.\theta) = a_0{}^l + b_0{}^l t + \sum_{h=1}^{\infty}\left(\frac{Sinh\left(\frac{h\pi}{\beta}(t-t_4)\right)}{Sinh\left(\frac{h\pi}{\beta}(t_3-t_4)\right)} a_h{}^l + \frac{Sinh\left(\frac{h\pi}{\beta}(t-t_3)\right)}{Sinh\left(\frac{h\pi}{\beta}(t_4-t_3)\right)} b_h{}^l\right). Cos\left(\frac{h\pi}{\beta}(\theta-\theta_l)\right) \tag{19}$$

where m is a positive integer and the coefficients, $a_0{}^l$, $b_0{}^l$, $a_h{}^l$ and $b_h{}^l$ are determined based on the continuity and interface conditions.

The continuity of the magnetic vector potential between the subdomain l and the regions m and I leads to

$$Al(t_4.\theta) = AI(t_5.\theta) \quad \text{for} \quad \theta_l \le \theta \le \theta_l + \beta \tag{20}$$

$$Al(t_3.\theta) = Am(t_4.\theta) \quad \text{for} \quad \theta_l \le \theta \le \theta_l + \beta \tag{21}$$

Interface condition (20) gives

$$a_0{}^l = \frac{1}{\beta}\int_{\theta_l}^{\theta_l+\beta} AI(t_5.\theta).d\theta \tag{22}$$

$$b_m{}^l = \frac{2}{\beta}\int_{\theta_l}^{\theta_l+\beta} AI(t_5.\theta). Cos\left(\frac{h\pi}{\beta}(\theta-\theta_l)\right).d\theta \tag{23}$$

Interface condition (21) gives

$$a_0{}^l + \ln\left(\frac{R_5}{R_6}\right) b_0{}^l = \frac{1}{\beta}\int_{\theta_l}^{\theta_l+\alpha} Am(t_4.\theta).d\theta \tag{24}$$

$$a_h{}^l = \frac{2}{\beta}\int_{\theta_l}^{\theta_l+\beta} Am(t_4.\theta). Cos\left(\frac{h\pi}{\beta}(\theta-\theta_l)\right).d\theta \tag{25}$$

3.3. Magnetic Vector Potential in the Air-gap Subdomain (Region I)

The Laplace's equation in the internal air-gap subdomain is given by

$$\frac{\partial^2 A_I}{\partial t^2} + \frac{\partial^2 A_I}{\partial \theta^2} = 0 \quad \text{for} \quad \begin{cases} t_5 \le t \le t_6 \\ 0 \le \theta \le 2\pi \end{cases} \tag{26}$$

where $\mathbf{t_5} = \mathbf{ln}\left(\frac{\mathbf{R_4}}{\mathbf{R_5}}\right)$ and $\mathbf{t_6} = \mathbf{0}$.

The general solution of (26) considering periodicity boundary conditions is obtained as

$$A_I(t.\theta) = \sum_{n=1}^{\infty}\left(\frac{1}{n}\frac{Cosh(n(t-t_6))}{Sinh(n(t_5-t_6))} a_n{}^I + \frac{1}{n}\frac{Cosh(n(t-t_5))}{Sinh(n(t_6-t_5))} b_n{}^I\right) Cos(n\theta) + \sum_{n=1}^{\infty}\left(\frac{1}{n}\frac{Cosh(n(t-t_6))}{Sinh(n(t_5-t_6))} c_n{}^I + \frac{1}{n}\frac{Cosh(n(t-t_5))}{Sinh(n(t_6-t_5))} d_n{}^I\right) Sin(n\theta) \tag{27}$$

where n is a positive integer.

The coefficients a_n^I, b_n^I, c_n^I and d_n^I are determined considering the continuity of magnetic vector potential between the internal air-gap subdomain I and the region I using a Fourier series expansion of interface condition (28) and (29) over the air-gap interval.

The continuity of the magnetic vector potential between the internal air-gap subdomain I and the regions l and k leads to

$$\left.\frac{\partial A_I}{\partial t}\right|_{t=t_5} = g(\theta) = \begin{cases} \left.\dfrac{\partial A_l}{\partial t}\right|_{t=t_4} & \text{for} \quad \theta_l \le \theta \le \theta_l + \beta \\ 0 & \text{elsewhere} \end{cases} \tag{28}$$

$$\left.\frac{\partial A_I}{\partial t}\right|_{t=t_6} = h(\theta) = \begin{cases} \left.\dfrac{\partial A_k}{\partial t}\right|_{t=t_7} & \text{for} \quad \theta_k \le \theta \le \theta_k + \gamma \\ 0 & \text{elsewhere} \end{cases} \tag{29}$$

Interface condition (28) gives

$$a_n^I = \frac{2}{2\pi}\int_{\theta_l}^{\theta_l+\beta} g(\theta).\mathrm{Cos}(n\theta).d\theta \tag{27}$$

$$c_n^I = \frac{2}{2\pi}\int_{\theta_l}^{\theta_l+\beta} g(\theta).\mathrm{Sin}(n\theta).d\theta \tag{28}$$

Interface condition (29) gives

$$b_n^I = \frac{2}{2\pi}\int_{\theta_k}^{\theta_k+\gamma} h(\theta).\mathrm{Cos}(n\theta).d\theta \tag{29}$$

$$d_n^I = \frac{2}{2\pi}\int_{\theta_k}^{\theta_k+\gamma} h(\theta).\mathrm{Sin}(n\theta).d\theta \tag{30}$$

3.4. Magnetic Vector Potential in the Rotor Slot-Opening Subdomain (Region k)

The Laplace's equation in the stator second inner slot-opening subdomain is given by

$$\frac{\partial^2 A_k}{\partial t^2} + \frac{\partial^2 A_k}{\partial \theta^2} = 0 \quad \text{for} \quad \begin{cases} t_7 \le t \le t_8 \\ \theta_k \le \theta \le \theta_k + \gamma \end{cases} \tag{34}$$

where $\mathbf{t_7 = \ln\left(\frac{R_3}{R_4}\right)}$ and $\mathbf{t_8 = 0}$.

Neumann BCs at the bottom and at each side of the slot are obtained as

$$\left.\frac{\partial A_{iI}}{\partial \theta}\right|_{\theta=\theta_k} = 0 \ \text{and} \ \left.\frac{\partial A_{iI}}{\partial \theta}\right|_{\theta=\theta_k+\gamma} = 0 \tag{35}$$

The general solution of (34) using the separation of variables method is given by

$$A_k(t.\theta) = a_0^k + b_0^k t + \sum_{h=1}^{\infty}\left(\frac{\mathrm{Sinh}\left(\frac{h\pi}{\gamma}(t-t_8)\right)}{\mathrm{Sinh}\left(\frac{h\pi}{\gamma}(t_7-t_8)\right)}a_h^k + \frac{\mathrm{Sinh}\left(\frac{h\pi}{\gamma}(t-t_7)\right)}{\mathrm{Sinh}\left(\frac{h\pi}{\gamma}(t_8-t_7)\right)}b_h^k\right).\mathrm{Cos}\left(\frac{h\pi}{\gamma}(\theta-\theta_k)\right) \tag{36}$$

where h is a positive integer and the coefficients, a_0^k, b_0^k, a_h^k and b_h^k are determined based on the continuity and interface conditions.

The continuity of the magnetic vector potential between the subdomain k and the regions j and I leads to

$$Ak(t_8.\theta) = Aj(t_9.\theta) \quad \text{for} \quad \theta_k \le \theta \le \theta_k + \gamma \tag{37}$$

$$Ak(t_7.\theta) = AI(t_6.\theta) \quad \text{for} \quad \theta_k \le \theta \le \theta_k + \gamma \tag{38}$$

Interface condition (37) gives

$$a_0^k = \frac{1}{\gamma}\int_{\theta_k}^{\theta_k+\gamma} Aj(t_9.\theta).d\theta \tag{39}$$

$$b_h^k = \frac{2}{\gamma}\int_{\theta_k}^{\theta_k+\gamma} Aj(t_9.\theta).\mathrm{Cos}\left(\frac{h\pi}{\gamma}(\theta-\theta_k)\right).d\theta \tag{40}$$

Interface condition (38) gives

$$a_0^k + \ln\left(\frac{R_3}{R_4}\right)b_0^k = \frac{1}{\gamma}\int_{\theta_i}^{\theta_i+\gamma} AI(t_6.\theta).d\theta \tag{41}$$

$$a_h^k = \frac{2}{\gamma}\int_{\theta_i}^{\theta_i+\gamma} AI(t_6.\theta).\mathrm{Cos}\left(\frac{h\pi}{\gamma}(\theta-\theta_k)\right).d\theta \tag{42}$$

3.5. Magnetic Vector Potential in the PM Subdomain (Region j)

The Poisson's equation in the stator PM subdomain is given by

$$\frac{\partial^2 A_j}{\partial t^2}+\frac{\partial^2 A_j}{\partial \theta^2}=-\mu_0\frac{M_\theta}{r} \quad \text{for} \begin{cases} t_9 \le t \le t_{10} \\ \theta_k \le \theta \le \theta_k+\gamma \end{cases} \tag{43}$$

where $\mathbf{t_9}=\mathbf{ln}\left(\frac{\mathbf{R_2}}{\mathbf{R_3}}\right)$ and $\mathbf{t_{10}}=\mathbf{0}$.

Neumann BCs at the bottom and at each side of the slot are obtained as

$$\left.\frac{\partial A_j}{\partial \theta}\right|_{\theta=\theta_k}=0 \quad \text{and} \quad \left.\frac{\partial A_j}{\partial \theta}\right|_{\theta=\theta_k+\gamma}=0 \tag{44}$$

The general solution of (40) is written as

$$A_j(t.\theta)=a_0^j+b_0^j t-\mu_0 M_j R_2 e^{-t}+\sum_{h=1}^{\infty}\left(\frac{\gamma}{h\pi}\frac{\mathrm{Cosh}\left(\frac{h\pi}{\gamma}(t-t_{10})\right)}{\mathrm{Sinh}\left(\frac{h\pi}{\gamma}(t_9-t_{10})\right)}{a_h}^j+\frac{\gamma}{h\pi}\frac{\mathrm{Cosh}\left(\frac{h\pi}{\gamma}(t-t_9)\right)}{\mathrm{Sinh}\left(\frac{h\pi}{\gamma}(t_{10}-t_9)\right)}{b_h}^j\right).\mathrm{Cos}\left(\frac{h\pi}{\gamma}(\theta-\theta_k)\right) \tag{45}$$

where $M_\theta=M_j=(-1)^i B_r/\mu_0$,l is a positive integer and the coefficients a_0^i, b_0^i, ${a_h}^j$ and ${b_h}^j$ are determined based on the continuity and interface conditions.

The continuity of the magnetic vector potential between the subdomain j and the region k and i leads to

$$\left.\frac{\partial A_j}{\partial t}\right|_{t=t_9}=\left.\frac{\partial A_k}{\partial t}\right|_{t=t_8} \quad \text{for} \quad \theta_k \le \theta \le \theta_k+\gamma \tag{46}$$

$$\left.\frac{\partial A_j}{\partial t}\right|_{t=t_{10}}=\left.\frac{\partial A_i}{\partial t}\right|_{t=t_{11}} \quad \text{for} \quad \theta_k \le \theta \le \theta_k+\gamma \tag{47}$$

Interface condition (46) gives

$$b_0^j+\mu_0 M_j R_2 e^{-t_9}=\frac{1}{\gamma}\int_{\theta_k}^{\theta_k+\gamma}\left.\frac{\partial A_k}{\partial t}\right|_{t=t_8}.d\theta \tag{48}$$

$${a_h}^j=\frac{2}{\gamma}\int_{\theta_k}^{\theta_k+\gamma}\left.\frac{\partial A_k}{\partial t}\right|_{t=t_8}.\mathrm{Cos}\left(\frac{h\pi}{\gamma}(\theta-\theta_k)\right).d\theta \tag{49}$$

Interface condition (44) gives

$$b_0^j+\mu_0 M_j R_2 e^{-t_{10}}=\frac{1}{\gamma}\int_{\theta_k}^{\theta_k+\gamma}\left.\frac{\partial A_i}{\partial t}\right|_{t=t_{11}}.d\theta \tag{50}$$

$${b_h}^j=\frac{2}{\gamma}\int_{\theta_k}^{\theta_k+\gamma}\left.\frac{\partial A_i}{\partial t}\right|_{t=t_{11}}.\mathrm{Cos}\left(\frac{h\pi}{\gamma}(\theta-\theta_k)\right).d\theta \tag{51}$$

3.6. Magnetic Vector Potential in the Subdomain (Region i)

The Laplace equation in the i-th rotor slot subdomain is given by

$$\frac{\partial^2 A_i}{\partial t^2}+\frac{\partial^2 A_i}{\partial \theta^2}=0 \quad \text{for} \quad \begin{cases} t_{11} \le t \le t_{12} \\ \theta_i \le \theta \le \theta_i+\delta \end{cases} \tag{52}$$

The general solution of (52) using the separation of variables method based on boundary conditions is

$$A_i(t.\theta)=\sum_{h=1}^{\infty}\left({a_h}^i\frac{\mathrm{Cosh}\left(\frac{h\pi}{\gamma}(t-t_{12})\right)}{\mathrm{Cosh}\left(\frac{h\pi}{\gamma}(t_{11}-t_{12})\right)}\right).\mathrm{Cos}\left(\frac{h\pi}{\delta}(\theta-\theta_i)\right) \tag{53}$$

where k is a positive integer and ${a_h}^i$ is an arbitrary constants.

The continuity of the magnetic vector potential between the i-th slot and the internal air-gap regions I leads to

$$Ai(t_{11}.\theta)=Aj(t_{10}.\theta) \quad \text{for} \quad \theta_i \le \theta \le \theta_i+\delta \tag{54}$$

Considering interface condition (54), the integration constants can be determined as

$${a_n}^i=\frac{2}{\gamma}\int_{\theta_i}^{\theta_i+\gamma}Aj(t_{10}.\theta).\mathrm{Cos}\left(\frac{h\pi}{\delta}(\theta-\theta_i)\right).d\theta \tag{55}$$

4. Performance Calculation and Model Evaluation

4.1. Performance Computation

The electromagnetic torque and cogging torque components are obtained using the Maxwell stress tensor in and expressed as

$$T_e = \frac{L_s}{\mu_0}\int_0^{2\pi} BI_r(t_e.\theta).BI_\theta(t_e.\theta).d\theta \qquad (56)$$

$$B_{I_r}(t_e.\theta) = -\frac{e^{t_e}}{R_2}\left(\sum_{n=1}^{\infty}\left(\begin{array}{c} a_n^I\frac{Cosh(n(t_e-t_6))}{Sinh(n(t_5-t_6))} \\ +b_n^I\frac{Cosh(n(t_e-t_5))}{Sinh(n(t_6-t_5))}\end{array}\right).Sin(n\theta) - \sum_{n=1}^{\infty}\left(\begin{array}{c} c_n^I\frac{Cosh(n(t_e-t_6))}{Sinh(n(t_5-t_6))} \\ +d_n^I\frac{Cosh(n(t_e-t_5))}{Sinh(n(t_6-t_5))}\end{array}\right).Cos(n\theta)\right) \qquad (57)$$

$$B_{I_\theta}(t_e.\theta) = -\frac{e^{t_e}}{R_2}\left(\sum_{n=1}^{\infty}\left(\begin{array}{c} a_n^I\frac{Sinh(n(t_e-t_6))}{Sinh(n(t_5-t_6))} \\ +b_n^I\frac{Sinh(n(t_e-t_5))}{Sinh(n(t_6-t_5))}\end{array}\right).Cos(n\theta) + \sum_{n=1}^{\infty}\left(\begin{array}{c} c_n^I\frac{Sinh(n(t_e-t_6))}{Sinh(n(t_5-t_6))} \\ +d_n^I\frac{Sinh(n(t_e-t_5))}{Sinh(n(t_6-t_5))}\end{array}\right).Sin(n\theta)\right) \qquad (58)$$

where L_s is the axial length of the motor and t_e is calculated by

$$t_e = \ln\left(\frac{R_4}{R_e}\right) \text{ with } R_e = (R_4+R_5)/2 \qquad (59)$$

For double layer winding, the phase flux vector is calculated by

$$\begin{bmatrix}\psi_a\\ \psi_b\\ \psi_c\end{bmatrix} = \begin{bmatrix}\psi1_a\\ \psi1_b\\ \psi1_c\end{bmatrix} + \begin{bmatrix}\psi2_a\\ \psi2_b\\ \psi2_c\end{bmatrix} \qquad (60)$$

where

$$\begin{bmatrix}\psi1_a\\ \psi1_b\\ \psi1_c\end{bmatrix} = \frac{N_c}{2}C_1^T[\varphi_{11} \quad \varphi_{12} \quad \varphi_{13} \quad \dots \quad \varphi_{1Q_2}] \qquad (61)$$

and

$$\begin{bmatrix}\psi2_a\\ \psi2_b\\ \psi2_c\end{bmatrix} = \frac{N_c}{2}C_2^T[\varphi_{21} \quad \varphi_{22} \quad \varphi_{23} \quad \dots \quad \varphi_{2Q_2}] \qquad (62)$$

For the stator slots, φ is given by

$$\varphi_{1i} = -\frac{2L_sR_4{}^2}{k_fS}\int_0^{\frac{\alpha}{2}}\int_0^{t_5} A_{m_i}(t.\theta).e^{-2t}.dt.d\theta \qquad (63)$$

$$\varphi_{2i} = -\frac{2L_sR_4{}^2}{k_fS}\int_{\frac{\alpha}{2}}^{\alpha}\int_0^{t_5} A_{m_i}(t.\theta).e^{-2t}.dt.d\theta \qquad (64)$$

The back-EMF of phase *a* is given by

$$E_a = \omega\frac{d\psi_a}{d\theta_r} \qquad (65)$$

where ω is the rotor angular speed and ψ_a is flux linkage per phase *a*.

The stator inductances (self-inductances) of phase *a* is given by

$$L = \frac{\psi_a}{I_a} \qquad (66)$$

where I_a is the peak current in phase *a*.

4.2. Model Evaluation

The investigated motor parameters are given in Table 1. A schematic diagram of the double layer winding of the motor is shown in Fig. 4. The 2-D FEM is applied on performance calculation of the motor. Magnetic field distribution in the motor is represented in Fig. 5. The fabricated spoke-type PM motor and experimental test setup are shown in Fig. 6 and Fig. 7, respectively.

Table 1 Parameters of the studied motor.

Symbol	Quantity Unit: angles (Mech. Degree) Dimensions (mm)	Value
R_1	Inner radius of the rotor inner slot	12.55
R_2	Inner radius of the rotor permanent magnet	18
R_3	Inner radius of the rotor slot-opening	30
R_4	Inner radius of the airgap	33.5
R_5	Inner radius of the stator slot-opening	35
R_6	Inner radius of the stator slot	36.5
R_7	Outer radius of the stator slot	49.5
R_8	Outer radius of the stator yoke	57.5
θ_i	Angular position of the first rotor inner slot	27
θ_k	Angular position of the first rotor slot-opening	22
θ_l	Angular position of the first stator slot-opening	18.77

θ_m	Angular position of the first stator slot	8.88
α	The stator slot angle	7.2
β	The stator slot-opening angle	2.45
γ	The rotor slot-opening angle	8.55
δ	The rotor inner slot angle	36
p	Pole pairs-number	4
Q_s	Number of stator slots	18
B_r	Remanence of the PM (T)	1.2
L_s	Axial length	48

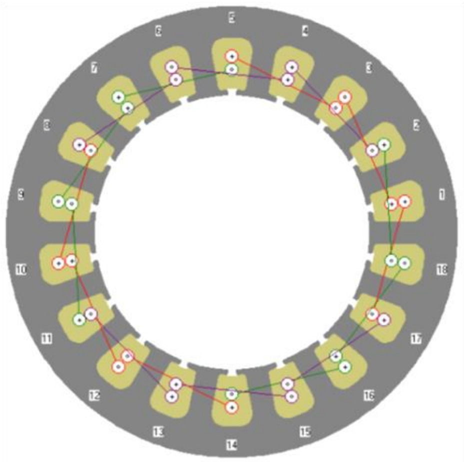

Fig. 4. A schematic diagram of the double layer winding of the investigated motor.

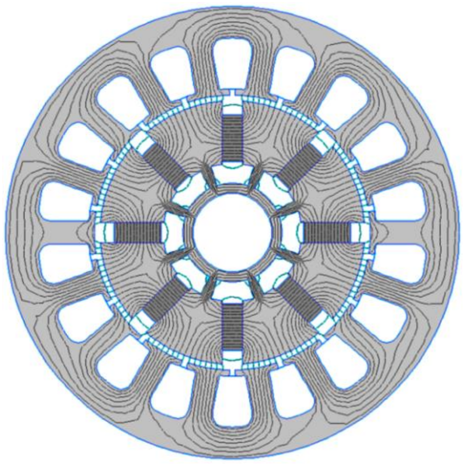

Fig. 5. Magnetic field distribution in 3-phases spoke-type PM motor.

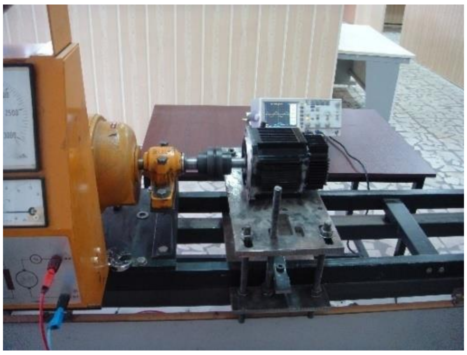

Fig. 6. Experimental test setup.

The motor performance results are compared analytically, numerically and experimentally in open circuit and full load conditions. The open circuit comparison of radial magnetic flux density and cogging torque waveforms are shown in Fig. 8 and Fig. 9, respectively.

The full load results at 6,000 rpm, including electromagnetic torque, back-EMF, self- and mutual inductances waveforms are shown in Fig. 8, Fig. 9, Fig. 10, Fig. 11, Fig. 12, and Fig. 13, respectively.

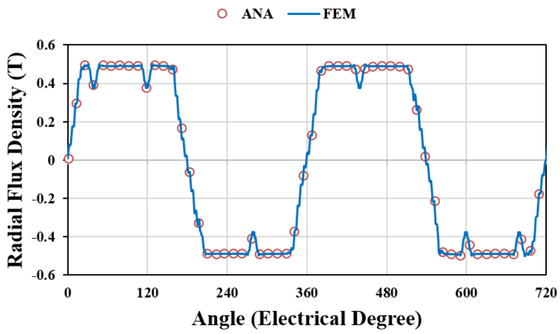

Fig. 7. Analytical and numerical comparison of radial magnetic flux density waveforms in mean radius of the studied motor.

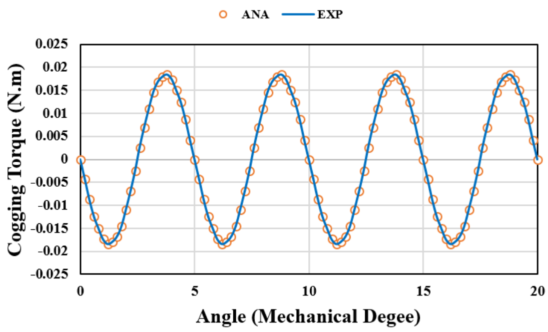

Fig. 8. Analytical and experimental comparison of cogging torque waveforms.

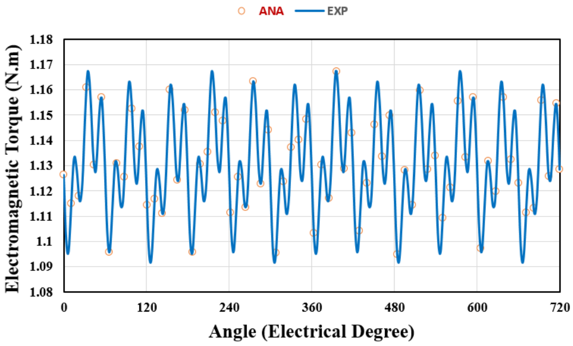

Fig. 9. Analytical and experimental comparison of electromagnetic torque waveforms at 6,000 rpm.

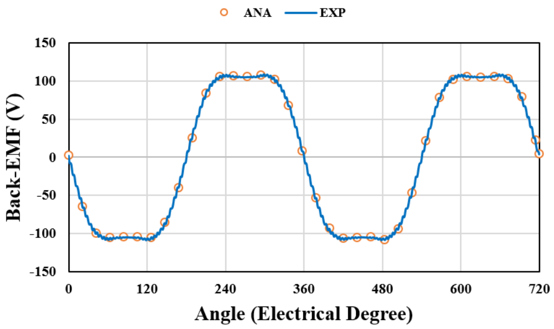

Fig. 10. Analytical and experimental comparison of phase back-EMF waveforms at 6,000 rpm.

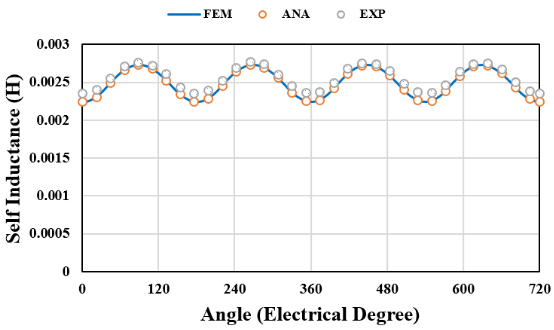

Fig. 11. Analytical and numerical comparison of phase self-inductance waveforms at 6,000 rpm.

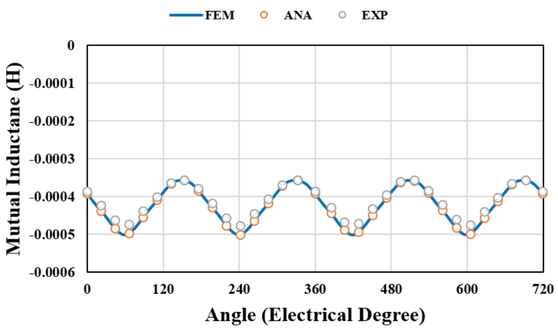

Fig. 12. Analytical and numerical comparison of mutual inductances waveforms at 6,000 rpm.

5. Conclusion

A 2-D analytical model for performance prediction in multiphase high-speed spoke-type PM machines considering slotting effects, magnetization orientation and winding layout has been developed in this paper. Fourier analysis method based on the subdomain technique is applied to derive analytical expressions for calculation of magnetic vector potential, magnetic flux density, electromagnetic torque, back-EMF and self- and mutual inductances in spoke-type PM machines. This model is applied for performance computation of a prototype spoke-type PM motor and the results of proposed model are verified thanks to FEM and experimental results.

References

[1] R. Benlamine, F. Dubas, C. Espanet, S.A. Randi, and D. Lhotellier "Design of an Axial-Flux Interior Permanent-Magnet Synchronous Motor for Automotive Application: Performance Comparison with Electric Motors Used in EVs and HEVs". In IEEE Vehicle Power and Propulsion Conference (VPPC), Coimbra, Portugal, 27-30 October 2014.

[2] S. Tohidi, "Analysis of Steady State Performance of Brushless Doubly Fed Machine", Journal of Iranian Association of Electrical and Electronics Engineers, Vol. 14, No. 1, pp. 119-125, 2017.

[3] K. Abbaszadeh, F. Saffar, "Numerical Modeling and Analysis Electromagnetic Forces in Oval Type Distribution Transformer", Journal of Iranian Association of Electrical and Electronics Engineers, Vol. 13, No. 1, pp. 123-134, 2016.

[4] Z. Q. Zhu and D. Howe, "Instantaneous magnetic-field distribution in brushless permanent-magnet dc motor, part III: Effect of slotting," IEEE Trans. Magn., Vol. 29, No. 1, pp. 143–151, Jan. 1993.

[5] M. Markovic, M. Jufer, and Y. Perriard, "Reducing the cogging torque in brushless dc motors by using conformal mappings," IEEE Trans. Magn., Vol. 40, No. 2, pp. 451–455, Mar. 2004.

[6] D. Zarko, D. Ban, and T. A. Lipo, "Analytical calculation of magnetic field distribution in the slotted air gap of a surface permanent-magnet motor using complex relative air-gap permeance," IEEE Trans. Magn., Vol. 42, No. 7, pp. 1828–1837, Jul. 2006.

[7] K. Boughrara, D. Zarko, R. Ibtiouen, O. Touhami, and A. Rezzoug, "Magnetic field analysis of inset and surface-mounted permanent- magnet synchronous motor using Schwarz-Christoffel transformation," IEEE Trans. Magn., Vol. 45, No. 8, pp. 3166–3168, Aug. 2009.

[8] E. Ilhan, B. L. J. Gysen, J. J. H. Paulides and E. A. Lomonova "Analytical Hybrid Model for Flux Switching Permanent Magnet Machines", IEEE Trans. Magn., Vol. 46, No. 6, pp. 1762-1765, June 2010.

[9] Y. Tang, T.E. Motoasca, J.J.H. Paulides, and E.A. Lomonova "Analytical modeling of flux-switching machines using variable global reluctance networks". In Electrical Machines (ICEM), 2012 XXth International Conference on, pp. 2792-2798, September 2012.

[10] W. Hua, G. Zhang, M. Cheng and J. Dong "Electromagnetic Performance Analysis of Hybrid-Excited Flux-Switching Machines by a Nonlinear Magnetic Network Model", IEEE Trans. Magn., Vol. 47, No. 10, pp. 3216-3219, October 2011.

[11] R. Benlamine, Y. Benmessaoud, F. Dubas and C. Espanet, "Nonlinear Adaptive Magnetic Equivalent Circuit of a Radial-Flux Interior Permanent-Magnet Machine Using Air-Gap Sliding-Line Technic," In IEEE Vehicle Power and Propulsion Conference (VPPC), Belfort, France, 11-14 December 2017.

[12] Y. Benmessaoud, F. Dubas, R. Benlamine, and M. Hilairet, "three-dimensional automatic generation magnetic equivalent circuit using mesh-based formulation," In 20th Int. Conf. on Electrical Machines and Systems (ICEMS), Sydney, NSW, Australia, 11-14 August 2017.

[13] Sh. Utegenova, F. Dubas, M. Janot, R. Glises, B. Truffart, D. Mariotto, P. Lagonotte, and Ph. Desevaux, "An Investigation Into the Coupling of Magnetic and Thermal Analysis for Wound-Rotor Synchronous Machine," IEEE Trans. Ind. Elec., Vol. 65, No. 4, pp. 3406-3416, 2018.

[14] Q. Gu and H. Gao, "Effect of slotting in PM electrical machines," Elect. Mach. Power Syst., Vol. 10, pp. 273–284, 1985.

[15] N. Boules, "Prediction of no-load flux density distribution in permanent magnet machines," IEEE Trans. Ind. Appl., Vol. IA-21, No. 3, pp. 633–643, Jul./Aug. 1985.

[16] B. Ackermann, and R. Sottek, "Analytical modeling of the cogging torque in permanent magnet motors," Elect. Eng., Vol. 78, No. 2, pp. 117–125, Mar. 1994.

[17] A. Radun, "Analytical calculation of the switched reluctance motor's unaligned inductance," IEEE Trans. Magn., Vol. 35, No. 6, pp. 4473–4481, Nov. 1999.

[18] K. F. Rasmussen, H. D. John, T. J. E. Miller, M. I. McGilp, and O. Mircea, "Analytical and numerical computation of air-gap magnetic field in brushless motors with surface permanent magnet," IEEE Trans. Magn., Vol. 36, No. 6, pp. 1547–1554, Nov./Dec. 2000.

[19] X. Wang, Q. Li, S. Wang, and Q. Li, "Analytical calculation of air-gap magnetic field distribution and instantaneous characteristics of brushless dc motors," IEEE Trans. Energy. Convers., Vol. 18, No. 3, pp. 386–391, Sep. 2003.

[20] Z. J. Liu and J. T. Li, "Analytical solution of air-gap field in permanent magnet motors taking into account the effect of pole transition over slots," IEEE Trans. Magn., Vol. 43, No. 10, pp. 3872–3882, Oct. 2007.

[21] Z. J. Liu, J. T. Li, and Q. Jiang, "An improved analytical solution for predicting magnetic forces in permanent magnet motors," J. Appl. Phys., Vol. 103, No. 7, 2008.

[22] Z. J. Liu and J. T. Li, "Accurate prediction of magnetic field and magnetic forces in permanent magnet motor using an analytical solution," IEEE Trans. Energy. Convers., Vol. 23, No. 3, pp. 717–726, Sep. 2008.

[23] P. Kumar, and P. Bauer, "Improved analytical model of a permanent magnet brushless dc motor," IEEE Trans. Magn., Vol. 44, No. 10, pp. 2299–2309, Oct. 2008.

[24] F. Dubas, and C. Espanet, "Analytical solution of the magnetic field in permanent-magnet motors taking into account slotting effect: No-Load vector potential and flux density calculation," IEEE Trans. Magn., Vol. 45, No. 5, pp. 2097-2109, May 2009.

[25] T. Lubin, S. Mezani, and A. Rezzoug, "Exact analytical method for magnetic field computation in the air gap of cylindrical electrical machines considering slotting effects," IEEE Trans. on Magn., Vol. 46, No. 4, pp. 1092-1099, 2010

[26] B. L. J. Gysen, E. Ilhan, K. J. Meessen, J. J. H. Paulides and E. A. Lomonova, "Modeling of Flux Switching Permanent Magnet Machines With Fourier Analysis", IEEE Trans. Magn.., Vol. 46, No. 6, pp. 1499-1502, June 2010.

[27] Z. Q. Zhu, L. J. Wu, and Z. P. Xia, "An accurate subdomain model for magnetic field computation in slotted surface-mounted permanent-magnet machines", IEEE Trans. Magn. Vol. 46, No 6, pp. 1100-1115, 2010.

[28] L. J. Wu, Z. Q. Zhu, D. Staton,, M. Popescu, and D. Hawkins, "An improved subdomain model for predicting magnetic field of surface-mounted permanent magnet machines accounting for tooth-tips", IEEE Trans. Magn., Vol. 7, No. 6, pp. 1693-1704, 2011.

[29] K. Boughrara, R. Ibtiouen, and T. Lubin, "Analytical prediction of magnetic field in parallel double excitation and spoke-type permanent-magnet machines accounting for tooth-tips and shape of polar pieces," IEEE Trans. Magn., Vol. 48, No. 7, pp. 2121-2137, 2012.

[30] D. Lin, P. Zhou, C. Lu, and S. Lin,: "Analytical prediction of cogging torque for spoke type permanent magnet machines", IEEE Trans. Magn., Vol. 48, No. 2, pp. 1035-1038, 2012.

[31] K. Boughrara, R. Ibtiouen, and F. Dubas, "Analytical Prediction of Electromagnetic Performances and Unbalanced Magnetic Forces in Fractional-Slot Spoke-Type Permanent-Magnet Machines," International Conference on Electric Machines (ICEM), Lausanne, Switzerland, 04-07 September 2016.

[32] P. X. Liang, F. Chai, Y. Li, and Y. L. Pei, "Analytical prediction of magnetic field distribution in spoke-type permanent magnet synchronous machines accounting for bridge saturation and magnet shape," IEEE Trans. Ind. Electron., Vol. 64, No. 5, pp. 3479-3488, 2017.

[33] Y. Zhou, H. S. Li, "Analytical Calculation and Optimization of Magnetic Field in Spoke-Type Permanent-Magnet Machines Accounting for Eccentric Pole-Arc Shape," IEEE Trans. Magn., Vol. 53, No. 9, pp. 01-07, 2017.

[34] K. Boughrara, T. Lubin, and R. Ibtiouen, "General subdomain model for predicting magnetic field in internal and external rotor multiphase flux-switching machines topologies," IEEE Trans. Magn., Vol. 49, No. 10, pp. 5310-5325, 2013.

[35] T.L. Tiang, D. Ishak, and M.K.M. Jamil, "Complete subdomain model for surface-mounted permanent magnet machines", In Energy Conversion (CENCON), 2014 IEEE Conference on, pp. 140-145, October 2014.

[36] Y. Zhou, H. S. Li, G. W. Meng, S. Zhou, and Q. Cao, "Analytical calculation of magnetic field and cogging torque in surface-mounted permanent-magnet machines accounting for any eccentric rotor shape," IEEE Trans. Ind. Electron., Vol. 62, No. 6, pp. 3438-3447, 2015.

[37] P-D. Pfister, X. Yin, and Y. Fang, "Slotted permanent-magnet machines: General analytical model of magnetic fields, torque, eddy currents, and permanent-magnet power losses including the Diffusion effect," IEEE Trans. Magn., Vol. 52, No. 5, 2016, Art. ID 8103013.

[38] X. Liu, H. Hu, J. Zhao, A. Belahcen, L. Tang, and L. Yang, "Analytical Solution of the Magnetic Field and EMF Calculation in Ironless BLDC Motor". IEEE Trans. Magn., Vol. 52, No. 2, pp.1-10, 2016.

[39] B. Dianati, H. Heydari, and S.A. Afsari, "Analytical Computation of Air-Gap Magnetic Field in a Viable Superconductive Magnetic Gear," IEEE Trans. Applied Superconductivity, Vol. 26, No. 6, pp. 1-12, 2016.

[40] R. L. J. Sprangers, J. J. H. Paulides, B. L. J. Gysen, and E. A. Lomonova, "Magnetic saturation in semi-analytical harmonic modeling for electric machine analysis," IEEE Trans. Magn., Vol. 52, No. 2, 2016, Art. ID 8100410.

[41] R. L. J. Sprangers, J. J. H. Paulides, B. L. J. Gysen, J. Waarma, and E. A. Lomonova, "Semi-analytical framework for synchronous reluctance motor analysis including finite soft-magnetic material permeability," IEEE Trans. Magn.., Vol. 51, No. 11, 2015, Art. ID 8110504.

[42] Z. Djelloul-khedda, K. Boughrara, F. Dubas, and R. Ibtiouen, "Nonlinear analytical prediction of magnetic field and electromagnetic performances in switched reluctance machines," IEEE Trans. Magn., Vol. 53, No. 7, 2017, Art. ID 8107311.

[43] Z. Djelloul-khedda, K. Boughrara, F. Dubas, A. Kechroud, and B. Souleyman, "Semi-analytical magnetic field predicting in many structures of permanent-magnet synchronous machines considering the iron permeability," IEEE Trans. Magn., Vol. 54, No. 7, 2018, Art. ID 8103921.

[44] Z. Djelloul-khedda, K. Boughrara, F. Dubas, A. Kechroud, and A. Tikellaline, "Analytical prediction of iron-core losses in flux-modulated permanent-magnet synchronous machines," IEEE Trans. Magn., Vol. 55, No. 1, 2019, Art. ID 63001112.

[45] F. Dubas, and K. Boughrara, "New scientific contribution on the 2-D subdomain technique in Cartesian coordinates: Taking into account of iron parts," Math. Comput. Appl., Vol. 22, No. 1, p. 17, 2017, DOI: 10.3390/mca22010017.

[46] F. Dubas, and K. Boughrara, "New Scientific Contribution on the 2-D Subdomain Technique in Polar Coordinates: Taking into Account of Iron Parts", Math. Comput. Appl., Vol. 22, No. 4, pp. 42, 2017, DOI: 10.3390/mca22040042.

[47] L. Roubache, K. Boughrara, F. Dubas, and R. Ibtiouen, "New subdomain technique for electromagnetic performances calculation in radial-flux electrical machines considering finite soft-magnetic material permeability," IEEE Trans. Magn., Vol. 54, No. 4, 2018, Art. ID 8103315.

[48] M. Ben Yahia, K. Boughrara, F. Dubas, L. Roubache, and R. Ibtiouen, "Two-Dimensional Exact Subdomain Technique of Switched ReluctanceMachines with Sinusoidal Current Excitation," Math. Comput. Appl., Vol. 23, No. 4, p. 59, 2018, DOI: 10.3390/mca23040059.

[49] K. Boughrara, F. Dubas, and R. Ibtiouen, "2-D exact analytical method for steady-state heat transfer prediction in rotating electrical machines," IEEE Trans. Magn., Vol. 54, No. 9, 2018, Art. ID 8104519.

[50] L. Roubache, K. Boughrara, F. Dubas, and R. Ibtiouen, "Elementary subdomain technique for magnetic field calculation in rotating electrical machines with local saturation effect," Int. J. Comput. Math. Electr. Electron. Eng., Vol. 38, No. 1, pp. 24-45, 2018, DOI:10.1108/COMPEL-11-2017-0481.

[51] B. Gaussens, E. Hoang, O. de la Barriere, J. Saint-Michel, and M. Gabsi, "Analytical Approach for Air-gap Modeling of Field-Excited Flux- Switching machine: No-load Operation," IEEE Trans. Magn., Vol. 48, No. 9, pp. 2505-2517, 2012.

[52] B. Gaussens, E. Hoang, O. de la Barriere, J. Saint-Michel, P. Manfe, M. Lecrivain, and M. Gabsi, "Analytical Armature Reaction Field Prediction in Field-Excited Flux-Switching Machines using an Exact Relative Permeance Function," IEEE Trans. Magn., Vol. 49, No. 1, pp.628-641, 2013.